Journal of Hazardous Materials 418 (2021) 126347

Contents lists available at ScienceDirect

Journal of Hazardous Materials

journal homepage: www.elsevier.com/locate/jhazmat

Research Paper

Superior removal of As(III) and As(V) from water with Mn-doped β-FeOOH nanospindles on carbon foam

Bing Yan [a,c,*], Tian Liang [b], Xiaohui Yang [b], Ashok J. Gadgil [c,**]

[a] School of Environmental Studies, China University of Geosciences, Wuhan 430074, PR China
[b] Faculty of Materials Science and Chemistry, China University of Geosciences, Wuhan 430074, PR China
[c] Department of Civil and Environmental Engineering, University of California, Berkeley, CA 94720-1710, USA

ARTICLE INFO

Editor: Dr. H. Artuto

Keywords:
Arsenic removal
Monolith
Manganese doping
FeOOH
Oxidation-adsorption

ABSTRACT

Arsenic pollution of water is one of the severest environmental challenges threatening human health. Iron-based nanomaterials have been demonstrated effective in arsenic removal. However, they generally suffer from low removal efficiency towards highly toxic As(III), loss of active sites owing to agglomeration, and poor reusability. Herein, we report a carbonized melamine foam supported Mn(IV)-doped β-FeOOH nanospindles(CF@Mn-FeOOH NSp) for tackling the technical hurdles. The designed CF@Mn-FeOOH NSp appears as a free-standing monolith through a low-cost and straightforward hydrothermal method. The atomic-scale integration of Mn(IV) into β-FeOOH enables an *oxidation-adsorption* bifunctionality, where Mn(IV) serves as oxidizer for As(III) and Fe(III) acts as adsorber for As(V). The maximal adsorption capacity for As(V) and As(III) can reach 152 and 107 mg g^{-1}, respectively. Meanwhile, As in simulated high arsenic groundwater can be decreased to below 10 μg L^{-1} within 24 h. By simple "filtrating-washing", 85% and 82% of its initial adsorption capacity for As(V) and As(III) can be easily recovered even after 5-cycles reuse. Kinetics and isotherm adsorption study indicate that the arsenic adsorption behavior is mainly through chemical bonding during single-layer adsorbing process. The as-prepared CF@Mn-FeOOH offers a scalable, efficient, and recyclable solution for arsenic removal in groundwater and wastewater from mines and industry.

1. Introduction

The maximum contaminant limit of arsenic in drinking water proposed by World Health Organization (WHO-MCL) is 10 μg L^{-1} (Muthu Prabhu et al., 2019; Jain et al., 2009). However, high arsenic contamination of groundwater used for drinking is widely distributed worldwide (Rodriguez-Lado et al., 2013; Habuda-Stanic and Nujic, 2015). The inappropriate disposal of arsenic wastewater from mines and industry (usually at concentrations of tens of mg L^{-1} and mainly as As(III)) continues to contaminate the drinking water (Egal et al., 2009; Ahoranta et al., 2016). Therefore, it is extremely important and urgent to develop an effective technology to reduce arsenic concentration.

Numerous technologies, including adsorption (Yan et al., 2016), coagulation-precipitation (Matsui et al., 2017), biological degradation (Tian et al., 2012; Lin et al., 2018), and ion exchange (Ortega et al., 2017) are currently applied to remove arsenic from water. Adsorption, owing to its ease of operation, low-cost, high treatment efficiency, and low secondary pollution (Wong et al., 2017), is considered as one of the most attractive approaches. FeOOH is the mostly studied adsorber for arsenic in water for its excellent adsorption capacity towards arsenate (As(V)) (Fu et al., 2017; Peng et al., 2013; Zhang et al., 2007). However, FeOOH has limited ability to remove arsenite (As(III)), which is 60 times toxicity higher than As(V) (Feng et al., 2012; Shan and Tong, 2013). Thus, external oxidants are often utilized to transform As(III) to less-toxic As(V) for subsequent capture and removal by FeOOH in application. Since As(III) is the predominant As species in many areas of high arsenic groundwater (Lien and Wilkin, 2005; Sorg et al., 2014), adding oxidants in groundwater remediation will inevitably change the water environment and cause secondary pollution (Vogelin and Hug, 2003). Therefore, to synthesize iron-manganese binary oxide with dual function of "oxidation-adsorption" is usually adopted to solve this problem, where Mn plays as an intrinsic oxidant to oxidize As(III) to As (V) (Shan and Tong, 2013; McCann et al., 2018; Zhang et al., 2012; Zhang et al., 2007), which can be more readily adsorbed on the

* Corresponding author at: School of Environmental Studies, China University of Geosciences, Wuhan 430074, PR China.
** Corresponding author.
E-mail addresses: yanbing@cug.edu.cn (B. Yan), ajgadgil@berkeley.edu (A.J. Gadgil).

https://doi.org/10.1016/j.jhazmat.2021.126347
Received 22 March 2021; Received in revised form 23 May 2021; Accepted 4 June 2021
Available online 7 June 2021

neighboring FeOOH. This in-situ process avoids the secondary pollution caused by the addition of external oxidants. However, Mn, Fe, and O cannot be distributed evenly in iron-manganese binary oxide materials prepared via traditional methods (physical mixing or co-precipitation), which leads to partial shielding between active sites and results in inferior arsenic removal performance (Tresintsi et al., 2013).

Atomic-scale doping of Mn(IV) into the FOOH lattice can effectively expose active sites and facilitate the in-situ “oxidation-adsorption”, contributing to a high performance of As adsorption (Tresintsi et al., 2013; Pinakidou et al., 2016). In light of this, a hydrothermal preparation of Mn-doped β-FeOOH (Mn-FeOOH) was proposed. The atomic-scale doping can construct a single-phase Mn(IV)-FeOOH nanospindles, which promotes the homogeneous distribution of the dual active center of "oxidation Mn(IV)-adsorption Fe(III)", maximizing its arsenic oxidation and adsorption capability. Further, considering the common drawbacks of agglomeration and recycling difficulty as nanomaterial, the macroscopic porous scaffold of oxidized carbon foam are adopted to support nano-adsorbent of Mn(IV)-FeOOH nanospindles, which enables the composite to be recycled easily through a facile “filtrating-washing” process, overcoming the drawback of conventional powdered Mn(IV)-FeOOH nanomaterial (Ge et al., 2017). Besides, the carbon foam is derived from the melamine foam (MF), which is a kind of commercial polymer that has low cost, high flexibility, and large-scale availability. At the same time, the porous structure of the scaffold provides plentiful channels for the mass transportation of As(III) to the dual-centers (oxidation Mn(IV)-adsorption Fe(III)), enhancing the adsorbing kinetics of As.

In this study, we propose the hydrothermal preparation of a free-standing composite of Mn-FeOOH assembled on oxidized carbon foam (CF@Mn-FeOOH), which exhibits excellent adsorbing capacity towards both As(V) and As(III). Using dosage as 0.5 g L^{-1}, it can reduce As(III) and As(V) from 1 mg L^{-1} to below 10 μg L^{-1} (WHO-MCL) within 24 h and 12 h, respectively, exceeding the most common iron-based adsorbents (Feng et al., 2012; Shan and Tong, 2013; McCann et al., 2018; Zhang et al., 2012, 2007, 2013; Tresintsi et al., 2013; Chang et al., 2009; Chen et al., 2013; Gupta and Ghosh, 2009; Shevade and Ford, 2004; Wu et al., 2012; Andjelkovic et al., 2015). The raw materials used for preparing the composite are all inexpensive and readily available ($12 kg^{-1} for MF), along with the straightforward preparing method and efficient arsenic adsorption performance, enabling CF@Mn-FeOOH to be a promising candidate for commercial application of arsenic removal.

2. Materials and methods

2.1. Materials

All chemicals used in this study were of analytical grade (Sinopharm Chemical Reagent Co., Ltd., China). Arsenic solutions were prepared by dissolving Na_2HAsO_4 and $NaAsO_2$ in deionized water, respectively. MF was provided by Kelinmei Company in China.

2.2. Synthesis of CF@Mn-FeOOH nanospindles

Carbon foam(CF) was derived from melamine foam (MF) via carbonization under N_2 (at 700 °C for 2 h, using a temperature ramp of 5 °C min^{-1}), and cutted into slabs (3 ×1.5 ×0.5 cm^3). The CF pieces were then acidized by 3 mol L^{-1} H_2SO_4 and heated at 120 °C for 1 h respectively. After that, the slabs were washed and dried ($T = 50$ °C) to acquire the oxidized CF.

Mn-FeOOH nanospindles was obtained by hydrothermal process in stock solution of 10.8 mmol $FeCl_3 6H_2O$(2.92 g), 0.54 mmol $MnCl_2 4H_2O$ (0.1068 g, 5% of the iron molar ratio), 32 mmol $NaNO_3$ (2.72 g), 0.1 mL HCl (37.5 wt%), 9.5 mL deionized water and 22.4 mL acetonitrile (C_2H_3N, >99%). Then the oxidized CF was put into the above solution and stirred for another 60 min and heated at 100 °C for 4 h to prepare CF@Mn-FeOOH NSp. A batch of CF@FeOOH NSps was separately prepared according to the above procedures without $MnCl_2 4H_2O$.

2.3. Characterization

The crystalline mineral composition was measured by X-ray diffraction (XRD, Bruker D8-FOCUS powder diffraction system). A Fourier transform infrared (FTIR) spectrometer (Nicolet iS50) in the range of 400–4000 cm^{-1} by means of the KBr pellet technique was used to record the FTIR spectra. Zeta potentials of the samples were measured by a Zeta potential analyzer (Nano ZS90, UK). Thermo Fisher ESCALAB 250Xi XPS was utilized for X-ray photoelectron spectroscopy (XPS). The morphology and nanostructure of the obtained samples were examined using field-emission scanning electron microscope (FE-SEM, Hitachi SU8010 at 10.0 kV). The Brunauer-Emmett-Teller (BET) specific surface area was measured using Micromeritics ASAP 2046 Analyzer, while the pore size distributions of the samples were calculated by adopting the Barrett-Joyner-Halenda (BJH) model.

2.4. Batch adsorption experiments

Batch adsorption experiments were performed at fixed temperature of 25 °C, with 0.5 g L^{-1} adsorbent dosage to study the effects of pH, reaction time, initial concentration of arsenic and co-existing competing anions on arsenic removal in synthetic As(V) and As(III) solution respectively. Suspension samples were adjusted to certain pH by using diluted HCl and NaOH solution (0.1 mol L^{-1}).

Adsorption isotherm experiments were carried out to determine the arsenic adsorption capacities of adsorbents in As(V) and As(III) solution with initial concentrations ranged from 1 to 500 mg L^{-1} at pH = 7. The adsorption kinetics were studied at pH= 7 for 24 h in 20 mL of 10 mg L^{-1} either As(V) or As(III) solution. To determine the effect of initial pH on arsenic removal, 0.5 g L^{-1} of adsorbent was introduced into arsenic solutions (with 20 mg L^{-1} of either As(III) or As(V)) for 24 h with different initial pH, which were adjusted to 2, 4, 6, 7, 8 and 10 respectively. The influences of co-existing competing anions as Cl^- (NaCl, 99.5%), HCO_3^- ($NaHCO_3$, >99%), SO_4^{2-} ($Na_2SO_4 \cdot 10H_2O$, >99%) and PO_4^{3-} (NaH_2PO_4, 99.5%) on arsenic adsorption were investigated at two ion concentrations (0.1 and 1 mmol L^{-1}) in 10 mg L^{-1} of either As(V) or As(III) solution.

The high concentrations of soluble As (>1 mg L^{-1}) were measured using inductively coupled plasma atomic emission spectrometry (ICP-AES), while the low concentrations (<1 mg L^{-1}) were determined by atomic fluorescence spectrometry (AFS). Aqueous As(V) and As(III) were separated by filtering the filtrate with As-speciation anion exchange cartridges(Meng X.G, 1998; Guo et al., 2008) before testing.

2.5. Oxidation-adsorption mechanism of CF@Mn-FeOOH study

In order to explore the function of Mn and Fe-OOH, and unravel the ‘oxidation-adsorption’ mechanism of the adsorbent, CF@Mn-FeOOH and CF@FeOOH were compared in the above batch experiments respectively. At the same time, lower concentration of As(III) and As(V) (1 mg L^{-1}), similar to geogenic high arsenic groundwater, were adopted to evaluate the feasibility for potential realistic application. To further clarify the adsorption mechanism of CF@Mn-FeOOH, As speciation in the residual solution was separated to As(III) and As(V) before AFS analysis (Yan et al., 2002).

2.6. Desorption and reusability experiment

To verify the reusability of the as-obtained materials for arsenic adsorption, the adsorbent was subjected to a five-cycle adsorption-desorption experiment with the same experimental parameters as described in Section 2.4 in 10 mg L^{-1} of either As(V) or As(III) solution. After each adsorption cycle, the adsorbent was filtered, washed with NaOH solution (0.1 mol L^{-1}) for 30 min, then rinsed with deionized

water, soaked in H_2SO_4 solution (0.05 mol L^{-1}) for 10 min, followed by washing and drying before reuse.

3. Results and discussion

The preparation process is displayed in Fig. 1. MF was first carbonized under N_2. After calcination, MF turned from white to black, with its volume shrank as well as a mass loss of 81.3%, owing to the thermal decomposition of the polymer. Since the thermolysis CF was hydrophobic, an acid pre-oxidation was further carried out to increase the hydrophilicity for the successive loading of FeOOH nanospindles. The objective of this process was to generate abundant oxygen-containing functional groups (such as carboxyl radical) on the CF (Ge et al., 2017), which are beneficial to the complexation between oxidized CF and metal ions (Fe^{3+} and Mn^{2+}). Subsequently, various reagents ($FeCl_3{\cdot}6H_2O$, $MnCl_2{\cdot}4H_2O$, $NaNO_3$, HCl, deionized water, and acetonitrile) were subjected to a hydrothermal reaction to assemble Mn doped FeOOH nanospindles onto the oxidized CF. During the hydrothermal process, the acidic environment forced Fe^{3+} to hydrolyze and homogeneously precipitate β-FeOOH (Music et al., 1998) on the complexation sites along the oxidized CF. Mn(II) was introduced and precipitated with β-FeOOH simultaneously as Mn-FeOOH, which then chemically anchored to CF, generating CF@Mn-FeOOH nanospindles (Nishida et al., 2018). After hydrothermal reaction, the total mass of the sample increased from 217 mg to 462 mg, with its color changed from black to brown.

3.1. Characterization of CF@Mn-FeOOH nanospindles

The SEM images in Fig. 2 show the morphologies and microstructures of the obtained samples. Fig. 2(a) displays the inter-connected and integral frame of the carbon foam made of carbon fibers, which is beneficial for the mass transfer of the ions in solution along the porous fibers. Fig. 2(b) shows the smooth surface of carbon fiber. Compared with Fig. 2(b), Fig. 2(c)–(f) exhibit a rough surface, indicating the loading of FeOOH and Mn-FeOOH nanospindles on the carbon fiber. It can be seen in Fig. 2(d) and (f) that the FeOOH and Mn-FeOOH nanospindles were homogeneously distributed on the surface of carbon fiber, with the diameter of about 100 nm and length of 1 μm. The numerous evenly-distributed Mn-FeOOH nanospindles provided abundant active sites for arsenic oxidation-adsorption. The EDS mapping images of the CF@Mn-FeOOH NSp shown in Fig. 2(g) and (h) display the homogeneous distribution of C, O, Fe and Mn element through the backbone of CF, suggesting that Mn-FeOOH nanospindles are evenly distributed on the carbon fiber, which further promotes the high-efficient adsorption of arsenic.

The crystal structure of the obtained samples was verified with XRD. Several typical peaks of CF@FeOOH and CF@Mn-FeOOH at 11.94°, 16.92°, 26.9°, 34.22°, 35.33°, 46.69°, and 56.22° are indexed to the planes of (110), (200), (130), (400), (211), (411), and (251) for β-FeOOH, respectively (JCPDS No.75-1594) (Piao et al., 2008). The four samples exhibit almost the same XRD pattern, suggesting that the Mn doping would not change the crystal structure of FeOOH. However, when compare the unit cell parameters of the four samples, a changing trade can be found that as Mn doping into the lattice of FeOOH, the a and b axis would be compressed, while the c axis was stretched (Table S1, Supporting Information). The XRD results demonstrate the single phase of Mn doped FeOOH and imply the uniform distribution of Mn on FeOOH at atomic scale.

BET and BJH analyses were employed to analyze the specific surface area and pore characteristics of the obtained samples as shown in Fig. 3 (b) and (c). The BET specific surface area of the samples (Table S2, Supporting Information) illustrates that the specific surface areas were as followed: Mn-FeOOH (45.10 m^2 g^{-1})> FeOOH (42.68 m^2 g^{-1}) > CF@Mn-FeOOH (32.40 m^2 g^{-1}) >CF@FeOOH (29.86 m^2 g^{-1}) > CF (3.67 m^2 g^{-1}). It can be concluded that the specific surface area mainly originated from FeOOH and Mn-FeOOH nanospindles. It can also be seen from BJH analyses that the micro/mesopores were mainly derived from FeOOH and Mn-FeOOH nanospindles. Thus, the decoration of oxidized CF with FeOOH and Mn-FeOOH nanospindles further enlarged the specific surface area of CF@FeOOH and CF@Mn-FeOOH, by exposing more active sites for arsenic adsorption.

3.2. Arsenic adsorption kinetics

Fig. 4(a)–(d) displays the time-dependent adsorption kinetic models fitting the adsorption behavior of CF@FeOOH and CF@Mn-FeOOH in 10 mg L^{-1} of arsenic solution. The specific fitting results are displayed in Table S3 (Supporting Information) and the detailed information can be found in Text S1 (Supporting Information). After compare the two models of pseudo-first order kinetics model and pseudo-second order kinetics model, it is manifest that the adjustment R^2 in the latter one are much higher for both adsorbents, indicating the adsorption behavior towards As(III) and As(V) is more in line with the pseudo-second-order kinetic model. This indicates the adsorptions of the two adsorbents were of chemisorption nature (Hong et al., 2011). As shown in Fig. 4, for As (V) adsorption, each of the two adsorbents reached more than 87% of its maximal possible As(V) content within 60 min. Further, the treated solution meets the demand for drinking of WHO-MCL (<10 μg L^{-1}) within 24 h, indicating that the two adsorbents possess excellent adsorption ability towards As(V) (Fig. S2, Supporting Information).

For As(III) adsorption, CF@FeOOH could reach 50% of its maximal adsorption capacity within 60 min, while CF@Mn-FeOOH showed a higher maximal adsorbing capacity as 72%. This can be ascribed to the fact that Mn(IV) could oxidize As(III) to As(V), which is more easily to adsorb by Fe(III). Under the experimental conditions, FeOOH dissociated into Fe^{3+} or FeO^+, and combined with As(III) to As(V) to form Fe-O-As chemical bond (Fu et al., 2017; Ge et al., 2017). In pH-neutral solution, As(V) ion cluster is larger than that of As(III) and exhibits electronegativity, resulting in well combination with Fe^{3+} or FeO^+. However, the bond formed between As(III) and Fe^{3+} or FeO^+ was much weaker than that of As(V), hindering the forming of a stable chemical bond, which then led to lower adsorption capacity (Kersten et al., 2014). The adsorption kinetic data indicate that FeOOH is more effective in adsorbing As(V) in aqueous solution than As(III), therefore doping Mn can increase its adsorption capacity towards As(III).

In order to verify the potential application of the adsorbent, a simulated high arsenic groundwater solution of arsenate and arsenite at 1 mg L^{-1} were used respectively. The process of As removal by CF@Mn-FeOOH was illustrated in Fig. 5(e). It is noticeable that the residual

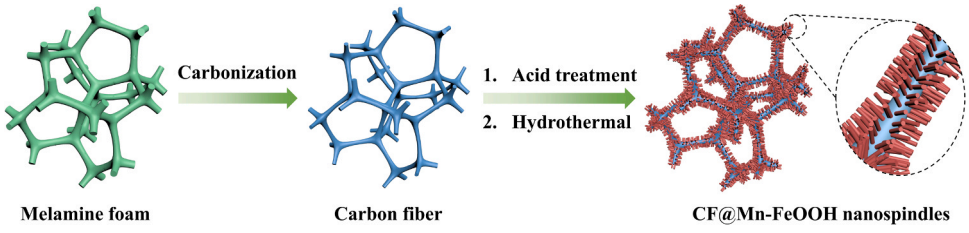

Fig. 1. Schematic illustration for the synthesis of CF@Mn-FeOOH nanospindles.

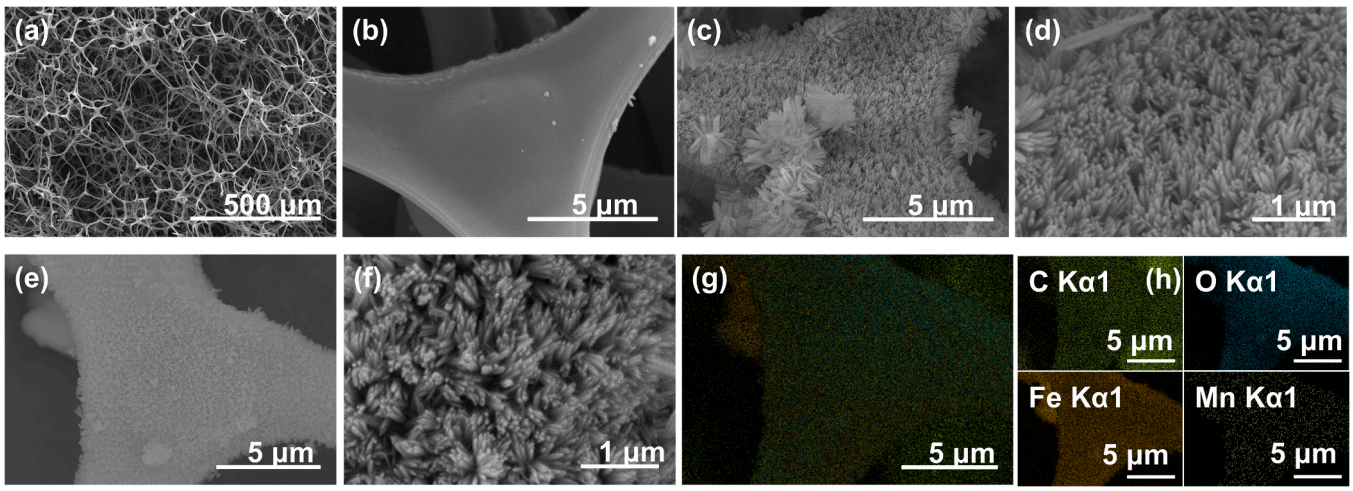

Fig. 2. SEM images of (a) & (b) oxidized carbon foam, (c) & (d) CF@FeOOH nanospindles, (e) &(f) CF@Mn-FeOOH nanospindles. Energy dispersive spectroscopy (EDS) mapping images of CF@Mn-FeOOH nanospindles are shown as (g) elements overlayer, and (h) C Kα1, O Kα1, Fe Kα1, and Mn Kα1.

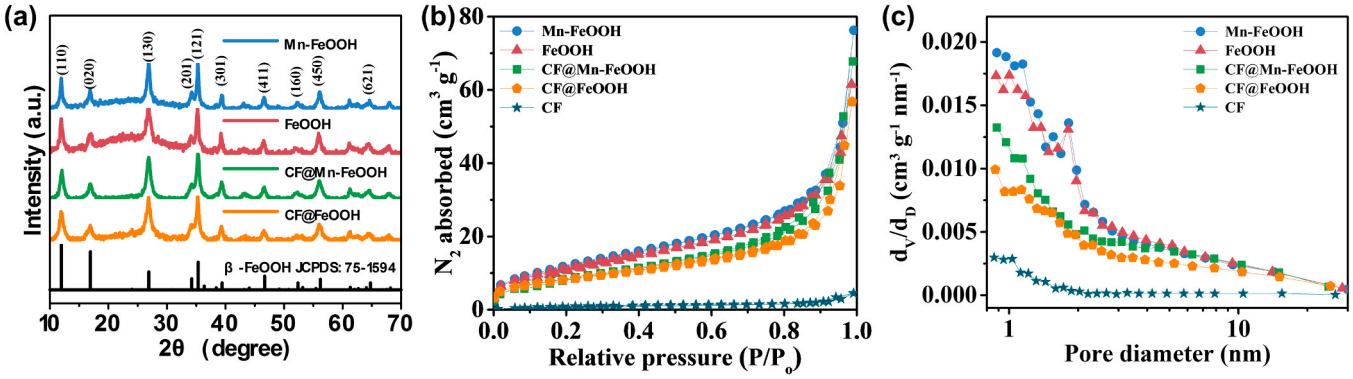

Fig. 3. (a) XRD patterns of CF@Mn-FeOOH, CF@FeOOH, Mn-FeOOH powder and FeOOH powder; (b) BET and (c) BJH analyses of Mn-FeOOH powder, FeOOH powder, CF@Mn-FeOOH, CF@FeOOH and melamine foam.

arsenic concentration was reduced sharply (around 70% decrease) in the first minute both for As(III) and As(V) solution. Furthermore, after adsorbing for 24 h, the total As concentration for As(III) and As(V) solution turned out to be 9.4 and 4.4 μg L^{-1}, respectively, both lower than the WHO-MCL for drinkable water. These results make the adsorbent more attractive in practice.

3.3. Arsenic adsorption isotherms

Arsenic adsorption isotherms of CF@FeOOH and CF@Mn-FeOOH for adsorbing As(V) and As(III) were examined and the corresponding results were illustrated in Fig. 5. All the isotherms were fitted with both Langmuir and Freundlich isotherm models, with detailed information shown in Text S2. The detailed parameters for the fitting results are displayed in Table S4 (Supporting Information), which reveal that both adsorbents obey a Langmuir isotherm model. Therefore, the adsorbing of arsenic was a single-layer adsorption process, indicating that the adsorption sites were homogeneously dispersed at the outer layer of the adsorbents (Fu et al., 2017).

In order to investigate the maximum adsorption capacity at equilibrium, the dosages of the adsorbents were fixed at 0.5 g L^{-1} even in solution of high arsenic concentration, hence the active sites of the adsorbents can be substantially occupied. It turned out that the maximal adsorption capacity for As(III) and As(V) by CF@Mn-FeOOH under 500 mg L^{-1} arsenic concentration were 107.3 and 152.5 mg g^{-1}, respectively, while for CF@FeOOH the data were 85.4 and 156.7 mg g^{-1}. It is manifest that CF@Mn-FeOOH had superior adsorption capacity towards As(III) than CF@FeOOH, but similar adsorption capability to As(V), which are in consistent of the results in adsorption kinetics study (3.2). This excellent adsorption capability towards As(III) and As(V) surpasses many other reported adsorbents (Zhang et al., 2007; Chen et al., 2013; Gupta and Ghosh, 2009; Shevade and Ford, 2004; Wang et al., 2016), which mainly benefited from the 3D interconnected network in CF@Mn-FeOOH contributing to the rapid ion transportation in aqueous solution, the homogeneous distribution of oxidative Mn(IV) helping to transform As(III) to As(V), as well as the ample active sites on the Mn-FeOOH nanospindles (Ge et al., 2017).

3.4. Effect of pH on arsenic adsorption

Initial pH of the solution may be one of the most important parameters that affects adsorption capacity of adsorbents. Hence, the zeta potential of CF@Mn-FeOOH under different pH and the influence of pH (from 2 to 10) on the removal of As(V) and As(III) by CF@FeOOH and CF@Mn-FeOOH was studied and the results were presented in Fig. 6. It can be seen that the zeta potential of the CF@Mn-FeOOH decreased as the pH value increased from 2 to 10 (Fig. 6(a)). Both adsorbents showed a larger adsorption capacity for both As(V) and As(III) at a lower pH, and the adsorption capacity declined as the pH increased (Fig. 6(b)). Meanwhile, the adsorption capacity for As(V) was higher than that for As(III) for a given adsorbent. The reason is that when the pH was low (<7), the hydroxyl groups on the surface of the adsorbents were protonated. Thus, the adsorbents surfaces were positively charged under acidic conditions, while under increasingly alkaline conditions, the

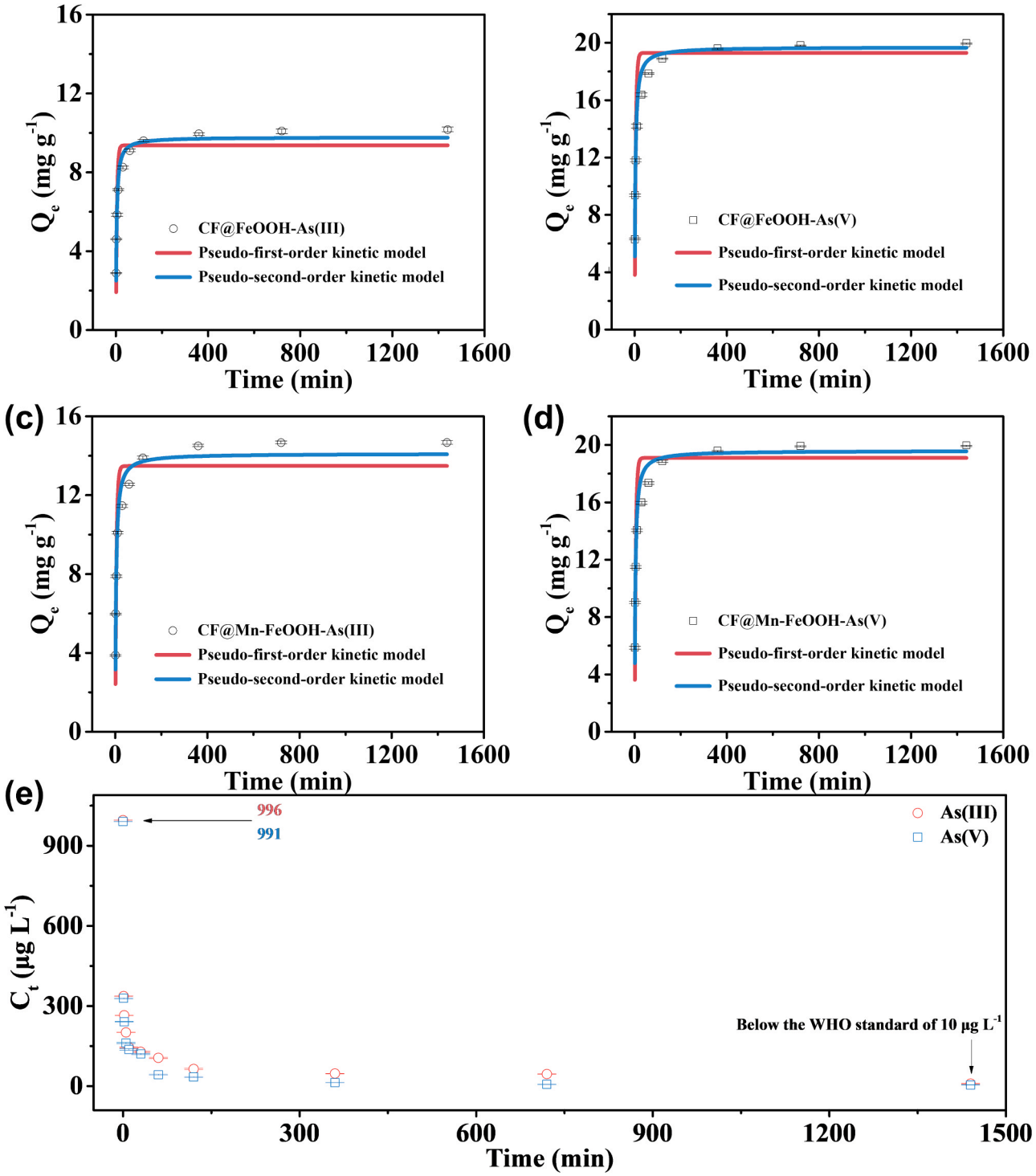

Fig. 4. (a–d) Adsorption kinetic model fittings of CF@FeOOH and CF@Mn-FeOOH adsorbing As in either 10 mg L^{-1} of As(III) or As(V) solution, and (e) As removal kinetic by CF@Mn-FeOOH in 1 mg L^{-1} of As(III) or As(V) solution.

adsorbents surfaces were negatively charged. Based on the Eh-pH diagram of arsenic (Wang and Mulligan, 2006), As(III) is stable in the form of H_3AsO_3 with pH from 4 to 9, while $H_2AsO_3^-$ is the stable form for pH > 9. As for As(V), $H_2AsO_4^-$ is the predominant species for pH from 2 to 7, while $HAsO_4^{2-}$ is the predominant form for pH> 7. In aqueous solution with the pH< 7, the positively charged adsorbents would uptake more of the anion $H_2AsO_4^-$ (As(V)) through electrostatic attraction, while adsorb less nonionic H_3AsO_3(As(III)). This explains why for the same kind of adsorbent, the adsorbed amount of As(V) was higher than that of As(III). When the pH value increased, the adsorbents would coordinate with OH^-, and their negatively charged surface would repulse the arsenic anions, resulting in a lower adsorption capacity. This is consistent with our experiment results that the adsorption capacity towards arsenic decreases with the pH value increases for the same kind of adsorbent.

When adsorbing As(V), CF@Mn-FeOOH and CF@FeOOH revealed little difference in adsorption capacity as shown in Fig. 6, with CF@FeOOH slightly larger than that of CF@Mn-FeOOH. This may be due to the fact that Mn atoms blocked some of the active sites of FeOOH

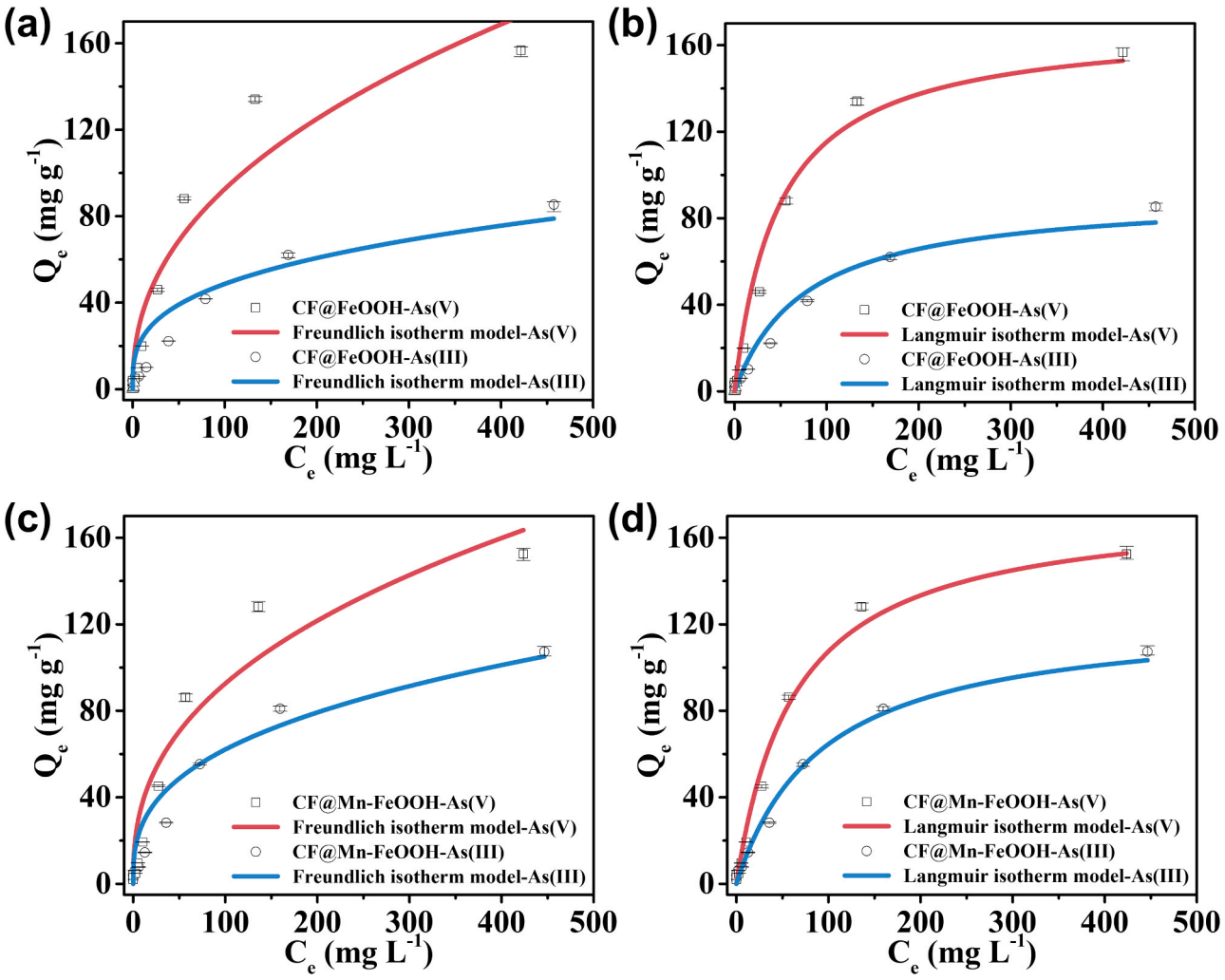

Fig. 5. Adsorption isotherm models fitting of (a) and (b) CF@FeOOH, and (c) and (d) CF@Mn-FeOOH, for adsorbing As(V) and As(III).

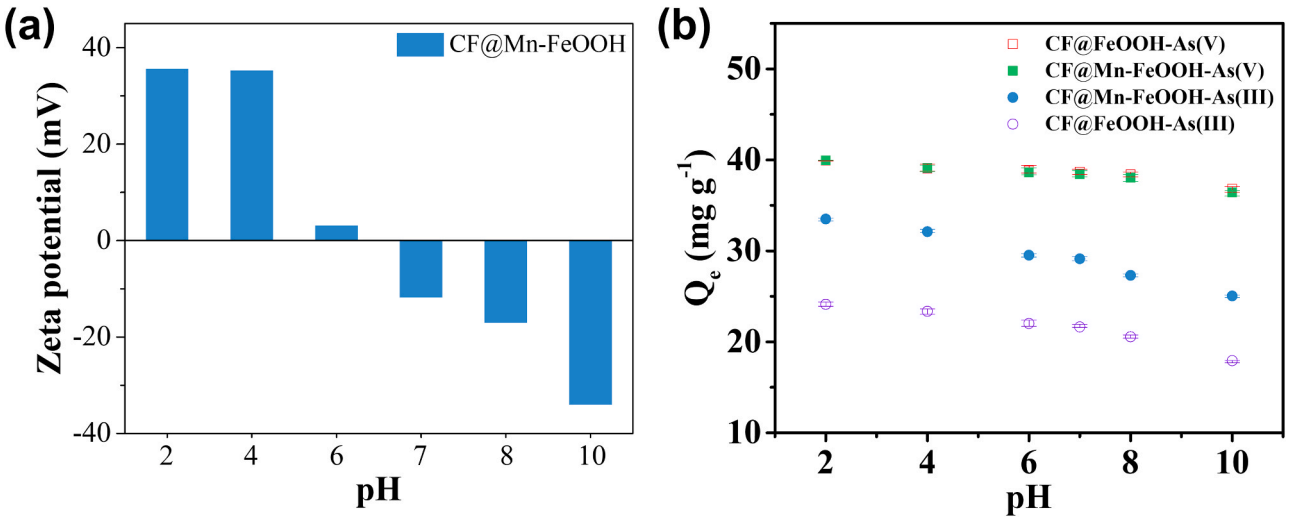

Fig. 6. (a) Zeta potential of CF@Mn-FeOOH under different pH, and (b) Influence of initial pH on the adsorption capacity of As(III) and As(V) by CF@FeOOH and CF@Mn-FeOOH.

in CF@Mn-FeOOH, thus adsorbed less As(V) than CF@FeOOH (Tresintsi et al., 2013). Another reason might be that the doped Mn decreased the mass of FeOOH and therefore decreased the adsorption ability of a unit mass of adsorbent. On the contrary, when adsorbing As(III), Mn(IV) played the irreplaceable role of oxidizing the hard-to-adsorbed As(III) to the easily adsorbed As(V), which was subsequently adsorbed by FeOOH.

In the process of adsorbing As(III), Mn(IV) cooperated with FeOOH and behaved much better than CF@FeOOH.

3.5. Effect of co-existing competing anions towards arsenic adsorption

The influences of four common co-existing competing anions (Cl^-, HCO_3^-, SO_4^{2-} and PO_4^-) in high arsenic groundwater (Xie et al., 2009) on the removal of As(V) and As(III) by CF@FeOOH and CF@Mn-FeOOH were investigated. Two different concentrations for each kind of ions (0.1 and 1 mmol L^{-1}) were conducted in the experiment. It is indicated in the results shown in Fig. S3 (Supporting Information), the influence of Cl^- and HCO_3^- (0.1 and 1 mmol L^{-1}) on the adsorption capacity of both As(III) and As(V) by the two adsorbents is almost unchanged. Similar negligible effect was observed for lower concentration of SO_4^{2-} (0.1 mmol L^{-1}). However, at higher concentration, SO_4^{2-} (1 mmol L^{-1}) depressed the adsorption of As(III) and As(V), especially for As(III). PO_4^{3-} manifested the greatest impact on the two adsorbents. The adsorption capacity of both adsorbents reduced drastically when PO_4^{3-} co-exist with arsenic in solution. A possible reason is that both SO_4^{2-} and PO_4^{3-} carry more charges, which cause them easily to coordinate with FeOOH (Ge et al., 2017). This results in the competition between the arsenic anions and the co-existing anions for the adsorption sites on FeOOH, thereby affecting the adsorption capacity of both adsorbents. Cl^- and HCO_3^- are smaller anions when compared to SO_4^{2-} and PO_4^{3-}, this render to their weak ability to compete with arsenic for sites on FeOOH. Hence, the effect of Cl^- and HCO_3^- towards the adsorption of arsenic by the two adsorbents was almost negligible.

3.6. Oxidation-adsorption mechanism of CF@Mn-FeOOH

According to the above results on arsenic removal by CF@Mn-FeOOH and CF@FeOOH with different experiment parameters including reaction time, initial concentration and solution pH, CF@Mn-FeOOH delivered better adsorption capacity towards As(V) and As(III). In order to verify the synergistic effect of Mn(IV) and FeOOH (where Mn (IV) oxidized As(III) to As(V), while FeOOH adsorbed both of As(III) and As(V)), FTIR and XPS analyses were utilized.

The FTIR analyses were utilized to verify the chemical reaction process between the adsorbent and adsorbate (Fig. 7(a)). The peak at around 1620 cm^{-1} was attributed to the deformation of water molecules, indicating there existed physisorbed water on the samples (Zhang et al., 2009). For the original CF@Mn-FeOOH spectrum, the peak around 1120 cm^{-1} can be assigned to the bending vibration of the hydroxyl group (Fe-OH) (Zhang et al., 2007). After adsorbing As(III), the peak of Fe-OH disappeared while a new peak that corresponded to the As-O stretching vibration appeared at around 820 cm^{-1} (Zhang et al., 2007). This indicated that As(III) was adsorbed onto CF@Mn-FeOOH and formed the Fe-O-As chemical bond, thus the Fe-OH disappeared while As-O appeared. It was also suggested that As was bound as a surface complex rather than a precipitated solid phase. The similar phenomena could also be seen in the spectra of CF@Mn-FeOOH adsorbing and desorbing As(V), where the peak of Fe-OH disappeared while As-O emerged, respectively.

Fig. 7(b)–(e) displayed the XPS data of full spectra, Fe 2p spectra, Mn 2p spectra, and As 3d spectra for the original CF@Mn-FeOOH and the samples after adsorbing/desorbing As(III)/As(V). In Fig. 7(b), the five samples exhibited the same symbolic peaks of C 1s, O 1s, Fe 2p and Mn 2p, with the samples adsorbing As(III)/As(V) showed additional As 3p peaks, in accordance with the adsorption process of arsenic. CF@Mn-FeOOH in Fig. 7(c) exhibited peaks at 711.1 and 724.8 eV, corresponding to Fe 2p3/2 and Fe 2p1/2, respectively. After the adsorption of As(III), the peaks shifted to higher energy of Fe 2p3/2 and Fe 2p1/2, locating at 711.6 and 725.4 eV, respectively. This may be attributed to the formation of Fe–O–As bonds in the arsenic adsorption process, during which the iron and arsenic chemically interact with each other (Fu et al., 2017; Ge et al., 2017). An even more positive shift can be observed after the adsorption of As(V), with peaks located at 711.7 and 725.5 eV corresponding to Fe 2p3/2 and Fe 2p1/2, respectively. The results indicate that the affinity between CF@Mn-FeOOH and As(V) was stronger than that of As(III), in line with the fact that the adsorption

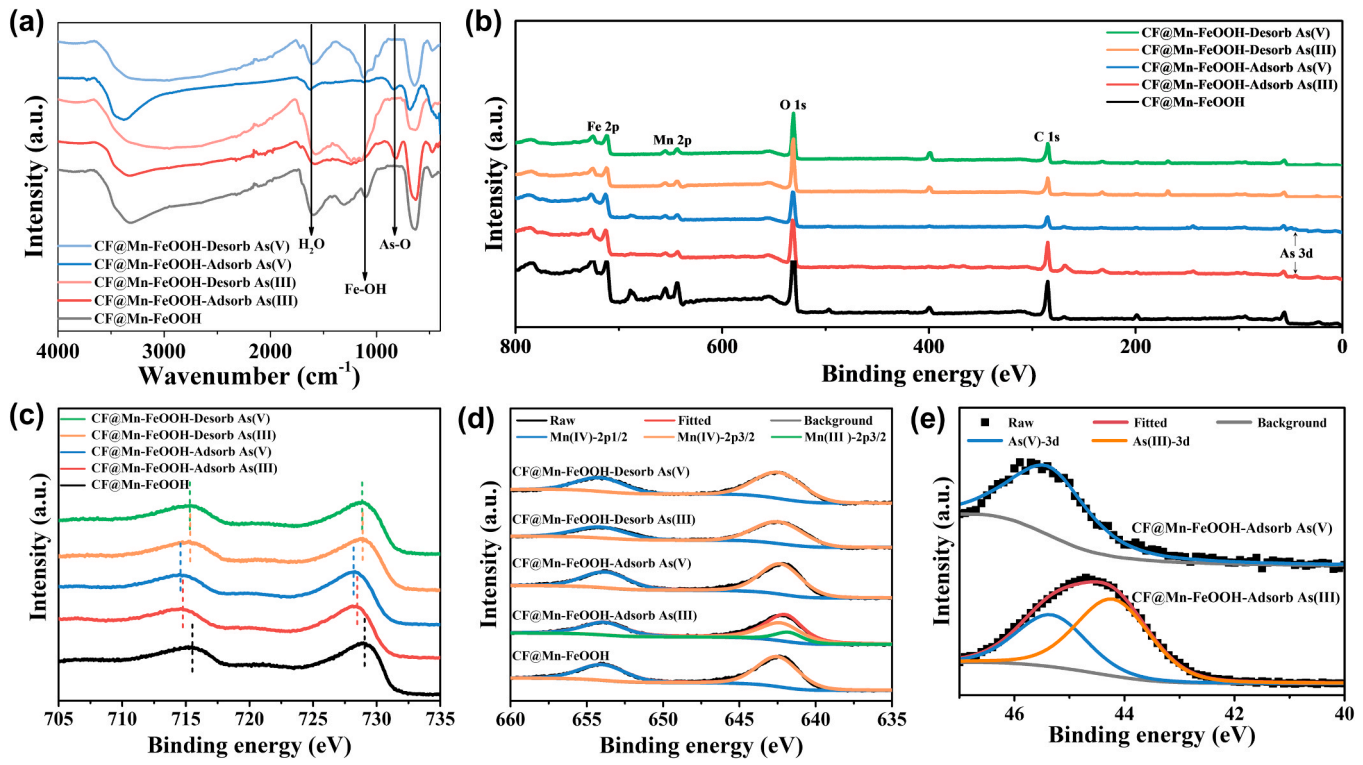

Fig. 7. (a) FTIR analyses of original CF@Mn-FeOOH and CF@Mn-FeOOH after adsorbing/desorbing As(III)/As(V). XPS analyses: (a) full spectra, (b) Fe 2p, (c) Mn 2p of original CF@Mn-FeOOH and CF@Mn-FeOOH after adsorbing/desorbing As(III)/As(V). (d) As 3d spectra of CF@Mn-FeOOH adsorbing As(III)/As(V).

capacity towards As(V) was higher than that of As(III). After the desorbing of As(III) and As(V), the peaks of Fe 2p3/2 and Fe 2p1/2 for both samples resumed to almost the same as that of original CF@Mn-FeOOH, demonstrating the dissociation of the Fe-O-As chemical bond.

The Mn 2p spectra of the three samples are shown in Fig. 7(d). The Mn 2p spectrum of the original CF@Mn-FeOOH can be deconvoluted into Mn(IV)−2p1/2 and Mn(IV)−2p3/2, situated at 654.1 and 642.4 eV, respectively. The Mn 2p spectrum of CF@Mn-FeOOH after adsorbing As (V) displays almost the same curve as that of original CF@Mn-FeOOH, demonstrating that there was no valence change of Mn during the adsorption process. For the Mn 2p spectrum of CF@Mn-FeOOH after adsorbing As(III), however, not only did the peak intensity decrease, but also the spectrum could be deconvoluted into three peaks, i.e.641.7, 642.4, and 654.1 eV for Mn(III)2p3/2, Mn(IV) 2p3/2, and Mn(IV) 2p1/2, respectively. It suggests that there was chemical reaction between Mn (IV) and As(III), probably Mn(IV) oxidized As(III) into As(V) and generated Mn(III), which is in consistent with the result that there are smaller contributions to the spectrum from Mn(IV), and that peaks of Mn (III) appears in the Mn 2p spectrum. The Mn 2p spectra of the samples after desorbing As(III) and As(V) were almost the same as that of original CF@Mn-FeOOH, indicating that Mn(III) was oxidized to Mn(IV) in the process of regeneration.

The As 3d spectra of CF@Mn-FeOOH after adsorbing As(III) and As (V) further proved the functionality of Mn(IV) oxidation (Fig. 7(e)). After adsorbing As(V), the As 3d spectrum of CF@Mn-FeOOH can only be deconvoluted into one peak locating at 45.4 eV that corresponded to As(V). Differently, after adsorbing As(III), the As 3d spectrum of CF@Mn-FeOOH can be deconvoluted into two peaks, i.e. 45.4 and 44.2 eV, attributing to As(V) and As(III), respectively (Zhang et al., 2007; Tang et al., 2017). It was manifest that the doped Mn(IV) within the CF@Mn-FeOOH could oxidize As(III) to more easily adsorbed As(V).

To further prove the oxidization of As(III) to As(V) during adsorbing process, and then explore the “oxidation-adsorption” behavior of CF@Mn-FeOOH towards As(III), As speciation was analyzed using AFS during arsenic removal by CF@Mn-FeOOH in 1 mg L^{-1} of arsenite solution, as shown in Fig. 8. It can be seen that the As(III) concentration reduced from 996 to 109 μg L^{-1} in the first 10 min, then slowly decreased to around 5 μg L^{-1} in the later adsorption stage (24 h). As(V) appeared at the very beginning of the process and peaked at 51 μg L^{-1} at the 5th minute and then gradually decreased to around 4.5 μg L^{-1}. It is suggested that As(III) started to transform to As(V) at the beginning, especially strongly within the first 5 min, proving the above conclusion. This can be ascribed to the numerous vacant active adsorption sites (Amstaetter et al., 2010) of CF@Mn-FeOOH in the first 10 min of the adsorbing process. Mn(IV) doped on the FeOOH nanospindles simultaneously oxidized the adsorbed As(III) to As(V), which was then in-situ adsorbed by FeOOH nanospindles, which is consistent in the XPS results above. At the same time, Mn(IV) also oxidized As(III) in the solution to As(V) (Tresintsi et al., 2013). FeOOH nanospindles kept adsorbing As(III) and oxidized As(V) from the solution as well as the in-situ oxidized As(V) transformed from As(III) on the nanospindles, resulting in less active adsorption sites and inferior adsorbing ability in the later stage. Therefore, As(III) and As(V) concentration in the residual solution decreased slowlier after the first 10 min.

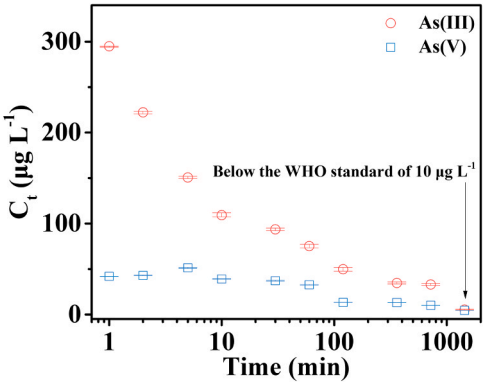

Fig. 8. The residual arsenic concentration separated to As(III) and As(V) species in As(III) solution when using CF@Mn-FeOOH to adsorb.

With the novel material described here, the introduction of Mn(IV) compensated for this deficiency by oxidizing As(III) into As(V). The synergistic effect of “oxidation (Mn(IV))-adsorption (FeOOH)” on the surfaces of CF@Mn-FeOOH results in the excellent adsorption capability towards both As(III) and As(V), showing much superior adsorption capacity when compared with CF@FeOOH.

3.7. Desorption and reusability study

In addition to the high adsorption capacity, when considering the practical application and realistic cost, it is also important for adsorbents to maintain their high ability to rapidly adsorb arsenic even after recycling for many times. The reusability of the two adsorbents is displayed in Fig. 9.

As seen from Fig. 9, the two adsorbents maintained a high value of maximum adsorption density (mg/g) of As(V) even after the first four regenerations. At the fifth cycle, the maximal adsorption density of CF@FeOOH and CF@Mn-FeOOH for As(V) were 17.3 and 16.9 mg g^{-1}, maintaining 86% and 85% of their initial maximum adsorption density.

Compared to As(V), the two adsorbents showed relatively smaller but more stable adsorption capacity towards As(III). CF@Mn-FeOOH (14.5 mg g^{-1}) was able to adsorb 41.7% more As(III) than CF@FeOOH (10.2 mg g^{-1}) in their initial adsorption. After five cycles, the maximal adsorption density of CF@Mn-FeOOH towards As(III) remained 82% of its initial value, while CF@FeOOH remained 72% of its initial value. Both adsorbents exhibited excellent reusability towards the adsorption of As(V) and As(III). The XRD results can also prove the superior stability and reusability of the adsorbents. After the 1st and 5th adsorbing/desorbing the As(III)/As(V), the XRD patterns of the CF@FeOOH and CF@Mn-FeOOH remained almost the same as their original samples (Fig. S4, Supporting Information).

Table S5 (Supporting Information) shows the comparison of adsorption capacity between our prepared CF@Mn-FeOOH and various other adsorbents. The performance of CF@Mn-FeOOH towards the adsorbing of As(III) and As(V) is seen to be superior to most of the reported adsorbents. Moreover, with low cost, CF@Mn-FeOOH is easy to prepare and to reuse, thus showing high potential for treating high arsenic contaminated water.

4. Conclusions

Arsenic pollution in groundwater has become a serious environmental issue, which demands advanced effective adsorbents for high-efficient arsenic removal. Herein, a free-standing composite of Mn doped β-FeOOH nanospindles decorated carbonized melamine foam (CF@Mn-FeOOH) has been prepared through a facile hydrothermal method, which displayed a "oxidation (Mn(IV))-adsorption (Fe(III))" bifunctionality and the characteristic of free standing. The composite is able to adsorb arsenic (both As(III) and As(V)) efficiently and can be easily reused. The oxidation and adsorption characteristics of CF@Mn-FeOOH regarding As(III), and As(V) have been systematically investigated. The maximal adsorption capacities for As(III) and As(V) were turned out to be 107 and 152 mg g^{-1}, respectively, under initial arsenic concentration of 500 mg L^{-1} at pH= 7. Meanwhile the simulated high arsenic groundwater can be treated to meet WHO-MCL for As within 24 h. The kinetic adsorption behavior of CF@Mn-FeOOH fitted well with the pseudo-second-order kinetic equation, suggesting the adsorbing of arsenic was mainly through chemical bonding; while the isotherm adsorption behavior was more consistent with the Langmuir isotherm

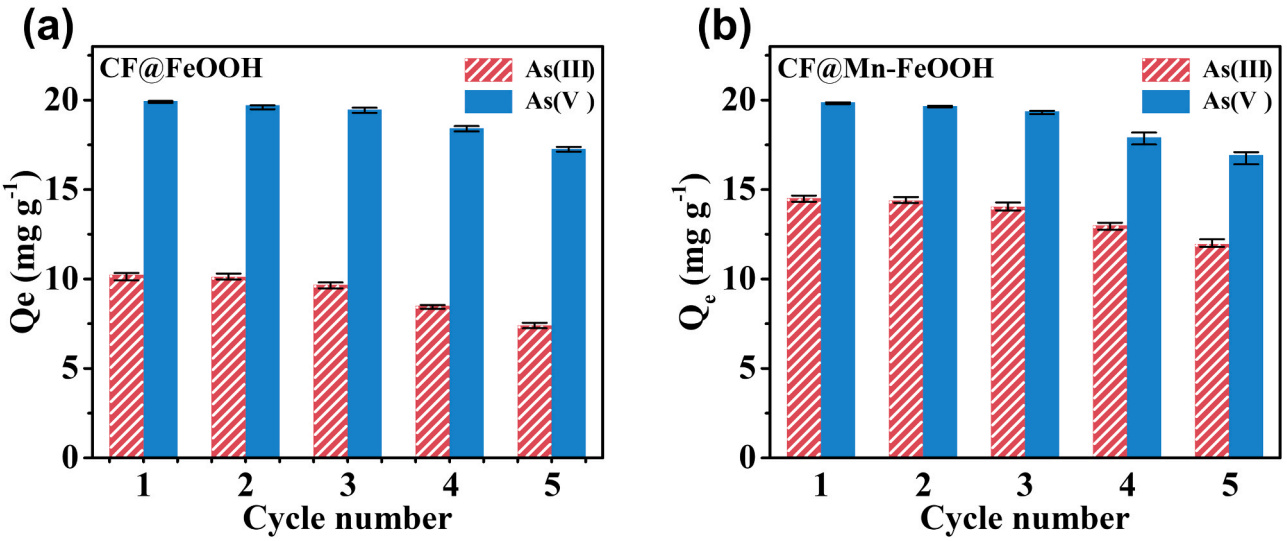

Fig. 9. Reusability of (a) CF@FeOOH and (b) CF@Mn-FeOOH towards the adsorption of As(III) and As(V).

model, demonstrating a monolayer adsorbing behavior. The adsorption capacity of CF@Mn-FeOOH towards arsenic decreased with the pH value. For reusability, this adsorbent was proved to maintain more than 80.0% of its initial removal capability (As(III): 82%, As(V): 85%, respectively) after five adsorption/desorption cycles, showing a good recycling stability. In summary, CF@Mn-FeOOH is a highly efficient adsorbent to remove arsenic (both As(III) and As(V)) from arsenic contaminated water and is a promising material for practical applications.

CRediT author contribution statement

Bing Yan and Ashok J. Gadgil conceived and designed the experiments. Tian Liang and Xiaohui Yang synthesized and characterized the materials. Bing Yan and Ashok J.Gadgil analyzed the results and wrote and revised the manuscript. The manuscript was written through the contributions of all authors.

Declaration of Competing Interest

The authors declare that they have no known competing financial interests or personal relationships that could have appeared to influence the work reported in this paper.

Acknowledgements

Bing Yan gratefully acknowledges the financial support of the National Natural Science Foundation of China (NSFC) Grants NO. 41807201. We also thank the support of China Scholarship Council (CSC) Grant NO. 201906415011 (Bing Yan) and NO. 201906410068 (Tian Liang).

Appendix A. Supporting information

Supplementary data associated with this article can be found in the online version at doi:10.1016/j.jhazmat.2021.126347.

References

Ahoranta, S.H., Kokko, M.E., Papirio, S., Ozkaya, B., Puhakka, J.A., 2016. Arsenic removal from acidic solutions with biogenic ferric precipitates. J. Hazard. Mater. 306, 124–132.

Amstaetter, K., Borch, T., Larese-Casanova, P., Kappler, A., 2010. Redox transformation of arsenic by Fe(II)-activated goethite (r-FeOOH). Environ. Sci. Technol. 44, 102–108.

Andjelkovic, I., Tran, D.N.H., Kabiri, S., Azari, S., Markovic, M., Losic, D., 2015. Graphene aerogels decorated with α-FeOOH nanoparticles for efficient adsorption of arsenic from contaminated waters. ACS Appl. Mater. Interfaces 7, 9758–9766.

Chang, F., Qu, J., Liu, H., Liu, R., Zhao, X., 2009. Fe-Mn binary oxide incorporated into diatomite as an adsorbent for arsenite removal: preparation and evaluation. J. Colloid Interface Sci. 338, 353–358.

Chen, B., Zhu, Z., Guo, Y., Qiu, Y., Zhao, J., 2013. Facile synthesis of mesoporous Ce-Fe bimetal oxide and its enhanced adsorption of arsenate from aqueous solutions. J. Colloid Interface Sci. 398, 142–151.

Egal, M., Casiot, C., Morin, G., Parmentier, M., Bruneel, O., Lebrun, S., Elbaz-Poulichet, F., 2009. Kinetic control on the formation of tooeleite, schwertmannite and jarosite by Acidithiobacillus ferrooxidans strains in an As(III)-rich acid mine water. Chem. Geol. 265, 432–441.

Feng, L., Cao, M., Ma, X., Zhu, Y., Hu, C., 2012. Superparamagnetic high-surface-area Fe3O4 nanoparticles as adsorbents for arsenic removal. J. Hazard. Mater. 217–218, 439–446.

Fu, D., He, Z., Su, S., Xu, B., Liu, Y., Zhao, Y., 2017. Fabrication of alpha-FeOOH decorated graphene oxide-carbon nanotubes aerogel and its application in adsorption of arsenic species. J. Colloid Interface Sci. 505, 105–114.

Ge, X., Ma, Y., Song, X., Wang, G., Zhang, H., Zhang, Y., Zhao, H., 2017. Beta-FeOOH nanorods/carbon foam-based hierarchically porous monolith for highly effective arsenic removal. ACS Appl. Mater. Interfaces 9, 13480–13490.

Guo, H., Yang, S., Tang, X., Li, Y., Shen, Z., 2008. Groundwater geochemistry and its implications for arsenic mobilization in shallow aquifers of the Hetao Basin, Inner Mongolia. Sci. Total Environ. 393, 131–144.

Gupta, K., Ghosh, U.C., 2009. Arsenic removal using hydrous nanostructure iron(III)-titanium(IV) binary mixed oxide from aqueous solution. J. Hazard. Mater. 161, 884–892.

Habuda-Stanic, M., Nujic, M., 2015. Arsenic removal by nanoparticles: a review. Environ. Sci. Pollut. Res. Int. 22, 8094–8123.

Hong, H.-J., Yang, J.-S., Kim, B.-K., Yang, J.-W., 2011. Arsenic removal behavior by Fe-Al binary oxide: thermodynamic and kinetic study. Sep. Sci. Technol. 46, 2531–2538.

Jain, A., Sharma, V.K., Mbuya, O.S., 2009. Removal of arsenite by Fe(VI), Fe(VI)/Fe(III), and Fe(VI)/Al(III) salts: effect of pH and anions. J. Hazard. Mater. 169, 339–344.

Kersten, M., Karabacheva, S., Vlasova, N., Branscheid, R., Schurk, K., Stanjek, H., 2014. Surface complexation modeling of arsenate adsorption by akageneite (β-FeOOH)-dominant granular ferric hydroxide. Colloid Surf. A 448, 73–80.

Lien, H.L., Wilkin, R.T., 2005. High-level arsenite removal from groundwater by zero-valent iron. Chemosphere 59, 377–386.

Lin, S., Yang, H., Na, Z., Lin, K., 2018. A novel biodegradable arsenic adsorbent by immobilization of iron oxyhydroxide (FeOOH) on the root powder of long-root Eichhornia crassipes. Chemosphere 192, 258–266.

Matsui, Y., Shirasaki, N., Yamaguchi, T., Kondo, K., Machida, K., Fukuura, T., Matsushita, T., 2017. Characteristics and components of poly-aluminum chloride coagulants that enhance arsenate removal by coagulation: detailed analysis of aluminum species. Water Res. 118, 177–186.

McCann, C.M., Peacock, C.L., Hudson-Edwards, K.A., Shrimpton, T., Gray, N.D., Johnson, K.L., 2018. In situ arsenic oxidation and sorption by a Fe-Mn binary oxide waste in soil. J. Hazard. Mater. 342, 724–731.

Meng, W.W., 1998. Speciation of Arsenic by Disposable Cartridges, Book of Posters of the Third International Conference on Arsenic Exposure and Health Effects.

Music, S., Santana, G.P., Smit, G., Gargd, V.K., Mossbauer, Fe, 1998. FT-IR and TEM investigations of Fe-oxide powders obtained from concentrated FeCl solutions. J. Alloy. Compd. 278, 291–301.

Muthu Prabhu, S., Park, C.M., Shahzad, A., Lee, D.S., 2019. Designed synthesis of sulfide-rich bimetallic-assembled graphene oxide sheets as flexible materials and self-tuning

adsorption cum oxidation mechanisms of arsenic from water. J. Mater. Chem. A 7, 12253–12265.
Nishida, N., Amagasa, S., Ito, H., Kobayashi, Y., Yamada, Y., 2018. Manganese-doped feroxyhyte nano-urchins produced by chemical methods. Hyperfine Interact. 239, 33.
Ortega, A., Oliva, I., Contreras, K.E., González, I., Cruz-Díaz, M.R., Rivero, E.P., 2017. Arsenic removal from water by hybrid electro-regenerated anion exchange resin/electrodialysis process. Sep. Purif. Technol. 184, 319–326.
Peng, F., Luo, T., Qiu, L., Yuan, Y., 2013. An easy method to synthesize graphene oxide–FeOOH composites and their potential application in water purification. Mater. Res. Bull. 48, 2180–2185.
Piao, Y., Kim, J., Na, H.B., Kim, D., Baek, J.S., Ko, M.K., Lee, J.H., Shokouhimehr, M., Hyeon, T., 2008. Wrap-bake-peel process for nanostructural transformation from beta-FeOOH nanorods to biocompatible iron oxide nanocapsules. Nat. Mater. 7, 242–247.
Pinakidou, F., Katsikini, M., Paloura, E.C., Simeonidis, K., Mitraka, E., Mitrakas, M., 2016. Monitoring the role of Mn and Fe in the As-removal efficiency of tetravalent manganese feroxyhyte nanoparticles from drinking water: an X-ray absorption spectroscopy study. J. Colloid Interface Sci. 477, 148–155.
Rodriguez-Lado, L., Sun, G., Berg, M., Zhang, Q., Xue, H., Zheng, Q., Johnson, C.A., 2013. Groundwater arsenic contamination throughout China. Science 341, 866–868.
Shan, C., Tong, M., 2013. Efficient removal of trace arsenite through oxidation and adsorption by magnetic nanoparticles modified with Fe-Mn binary oxide. Water Res. 47, 3411–3421.
Shevade, S., Ford, R.G., 2004. Use of synthetic zeolites for arsenate removal from pollutant water. Water Res. 38, 3197–3204.
Sorg, T.J., Chen, A.S., Wang, L., 2014. Arsenic species in drinking water wells in the USA with high arsenic concentrations. Water Res. 48, 156–169.
Tang, L., Feng, H., Tang, J., Zeng, G., Deng, Y., Wang, J., Liu, Y., Zhou, Y., 2017. Treatment of arsenic in acid wastewater and river sediment by Fe@Fe_2O_3 nanobunches: the effect of environmental conditions and reaction mechanism. Water Res 117, 175–186.
Tian, H., Zhuang, G., Ma, A., Jing, C., 2012. Arsenic interception by cell wall of bacteria observed with surface-enhanced Raman scattering. J. Microbiol. Methods 89, 153–158.
Tresintsi, S., Simeonidis, K., Estrade, S., Martinez-Boubeta, C., Vourlias, G., Pinakidou, F., Katsikini, M., Paloura, E.C., Stavropoulos, G., Mitrakas, M., 2013. Tetravalent manganese feroxyhyte: a novel nanoadsorbent equally selective for As (III) and As(V) removal from drinking water. Environ. Sci. Technol. 47, 9699–9705.
Vogelin, A., Hug, S.J., 2003. Catalyzed oxidation of Arsenic(III) by hydrogen peroxide on the surface of ferrihydrite: an in situ ATR-FTIR study. Environ. Sci. Technol. 37, 972–978.
Wang, S., Mulligan, C.N., 2006. Occurrence of arsenic contamination in Canada: sources, behavior and distribution. Sci. Total Environ. 366, 701–721.
Wang, S., Lan, H., Liu, H., Qu, J., 2016. Fabrication of FeOOH hollow microboxes for purification of heavy metal-contaminated water. Phys. Chem. Chem. Phys. 18, 9437–9445.
Wong, W., Wong, H.Y., Badruzzaman, A.B., Goh, H.H., Zaman, M., 2017. Recent advances in exploitation of nanomaterial for arsenic removal from water: a review. Nanotechnology 28, 042001.
Wu, Z., Li, W., Webley, P.A., Zhao, D., 2012. General and controllable synthesis of novel mesoporous magnetic iron oxide@carbon encapsulates for efficient arsenic removal. Adv. Mater. 24, 485–491.
Xie, X., Ellis, A., Wang, Y., Xie, Z., Duan, M., Su, C., 2009. Geochemistry of redox-sensitive elements and sulfur isotopes in the high arsenic groundwater system of Datong Basin, China. Sci. Total Environ. 407, 3823–3835.
Yan, L., Hu, S., Jing, C., 2016. Recent progress of arsenic adsorption on TiO_2 in the presence of coexisting ions: a review. J. Environ. Sci. -China 49, 74–85.
Yan, Xiu-Ping, Yin, Xue-Bo, He, Xi-Wen, Jiang, Y., 2002. Flow injection on-line sorption preconcentration coupled with hydride generation atomic fluorescence spectrometry for determination of (Ultra)trace amounts of Arsenic(III) and Arsenic(V) in natural water samples. Anal. Chem. 74, 2162–2166.
Zhang, G., Qu, J., Liu, H., Liu, R., Wu, R., 2007. Preparation and evaluation of a novel Fe-Mn binary oxide adsorbent for effective arsenite removal. Water Res 41, 1921–1928.
Zhang, G., Liu, H., Liu, R., Qu, J., 2009. Adsorption behavior and mechanism of arsenate at Fe-Mn binary oxide/water interface. J. Hazard. Mater. 168, 820–825.
Zhang, G., Liu, H., Qu, J., Jefferson, W., 2012. Arsenate uptake and arsenite simultaneous sorption and oxidation by Fe-Mn binary oxides: influence of Mn/Fe ratio, pH, Ca^{2+}, and humic acid. J. Colloid Interface Sci. 366, 141–146.
Zhang, G., Ren, Z., Zhang, X., Chen, J., 2013. Nanostructured iron(III)-copper(II) binary oxide: a novel adsorbent for enhanced arsenic removal from aqueous solutions. Water Res. 47, 4022–4031.
Zhang, J.S., Stanforth, R.S., Pehkonen, S.O., 2007. Effect of replacing a hydroxyl group with a methyl group on arsenic (V) species adsorption on goethite (alpha-FeOOH). J. Colloid Interface Sci. 306, 16–21.
Zhang, G.S., Qu, J.H, Liu, H.J, Liu, R.P., Li, G.-T., 2007. Removal mechanism of As(III) by a novel Fe-Mn binary oxide adsorbent: oxidation and sorption. Environ. Sci. Technol. 41, 4613–4619.